Journal of Organometallic Chemistry 694 (2009) 3160–3166

Contents lists available at ScienceDirect

Journal of Organometallic Chemistry

journal homepage: www.elsevier.com/locate/jorganchem

Chemically bonded metallic (Eu, Tb, Zn) hybrid materials through sulfide linkage: Molecular construction, physical characterization and photophysical properties

Bing Yan *, Kai Qian, Hai-Feng Lu

Department of Chemistry, Tongji University, Siping Road 1239, Shanghai 200092, China

ARTICLE INFO

Article history:
Received 25 March 2009
Received in revised form 7 May 2009
Accepted 11 May 2009
Available online 18 May 2009

Keywords:
Chemical bonded hybrid material
Sulfide linkage
Photophysical property

ABSTRACT

In this paper, a kind of aromatic carboxylic acid of sulfhydryl group (2-mercaptonicotinic acid) is modified with four silane crosslinking reagents (3-methacryloyloxypropyltrimethoxysilane (S_1), 3-glycidoxypropyltrimethoxysilane (S_2), 3-aminopropyltrimethoxysilane (S_3), and 3-(triethoxysilyl)propylisocyanate (S_4)) to achieve four new kinds of functionalized molecular bridge (P_i (i = 1–4)). Subsequently, four molecular bridges and lanthanides (europium and terbium) or zinc ions have been assembled via chemical bonds through a sol–gel (cohydrolysis and copolycondensation) process with inorganic precursor (tetraethoxysilane, TEOS), resulting in four novel series of chemically bonded hybrid materials which named as Ln (Zn)–M_i (i = 1–4). The coordinated bonding makes metal ions evenly dispersed in a stable hybrid system. The intramolecular energy transfer process between lanthanide ions and the molecular bridges take place within these molecular-based hybrids and especially the luminescent quantum efficiency of them are determined, suggesting that the hybrid material systems derived from different molecular bridges present different luminescence efficiencies.

1. Introduction

A wide range of hybrid organic–inorganic materials have attracted great scientific interest in order to combine various features together. They have great potential for many applications due to the synergy between the properties of these two different building blocks [1]. Many lanthanide complexes have been investigated thoroughly and applied in the luminescence hybrid materials owing to their long-lived excited-states characteristic and their especially efficient strong narrow-width emission band in the visible region [2,3]. Recently, the hybrid system of lanthanide organic complexes introduced in silica gel have already been found to have characteristic emission intensities compared with simple metal ions in inorganic hosts. In particular, rare-earth complexes with β-diketones, aromatic, carboxylic acids, and heterocyclic ligands in sol–gel derived host materials has been studied [4,5]. In order to solve the problem of concentration in the organic–inorganic hybrids, Sanchez and Ribot discussed the tailoring of diverse multifunctional materials induced by the mixture at the covalent bond level [6]. One is mechanical mixture and it seems impossible to solve the problem of clustering of emitting centers because only weak interactions (such as hydrogen bonding, van der Waals force or weak static effect) present between organic and inorganic components. Another is the type that has true connections: covalent bonding between the organic and inorganic moieties. Lately, research about the covalently bonded hybrids which can realize the possibility of tailoring the complementary properties of novel multifunctional advanced materials has emerged. Franville et al. have concentrated on the modification of pyridine-dicarboxylic acid or their derivatives and resulted in strong Eu^{3+} ions emissions due to efficient ligand-to-metal energy transfer [7]. Zhang and coworkers focused on modification of heterocyclic ligands including 1,10-phenanthroline and di-pyridine to construct molecular-based hybrids [8,9]. Our research group has also done a lot of work concerns the covalently bonded hybrids. We have successfully realized three paths to construct rare earth hybrid systems with chemical bonds. The first is to modify the amino groups of aniline using ester group of TESPIC [10,11]. The second path is to modify the carboxylic group of aromatic carboxylic acids using the amino group of amino-silane cross-linking [12–14]. The third is to modify the hydroxyl groups of hydroxyl compounds using ester group of TESPIC [15–17]. We assemble the above modified bridge ligands with rare earth ions and inorganic precursors (TEOS) to construct hybrid systems after the modification. Among all the synthetic methods, the sol–gel approach exhibits a wealth of unique characteristics, namely, convenience, low temperature, and versatility [18–22].

Based on the above research, it can be recognized that the critical step to prepare these hybrids is to synthesize a novel monomer as a covalent bridge that cannot only develop chelating effects that can bind to lanthanide ions but also act as precursors of inorganic network. Hence, the development of novel linkages between organic compounds and inorganic part is an important and active area. In this paper, sulfide bond was selected to construct the linkage. It is

* Corresponding author. Tel.: +86 21 65984663; fax: +86 21 65982287.
E-mail address: byan@tongji.edu.cn (B. Yan).

0022-328X/$ - see front matter © 2009 Elsevier B.V. All rights reserved.
doi:10.1016/j.jorganchem.2009.05.012

well know that the mercapto is active in many reactions [23–27]. So 2-mercaptonicotinic acid was chosen as the organic ligand at this time. It can react with 3-methacryloyloxypropyltrimethoxysilane, 3-glycidoxypropyltrimethoxysilane, 3-aminopropyltrimethoxysilane, and 3-(triethoxysilyl)propylisocyanate resulting in four new kinds of structural molecular bridge. Finally, four novel series of molecular hybrid materials are assembled by sol–gel process.

2. Experimental

2.1. Materials

Starting materials were purchased from Aldrich and were used as received. All normal organic solvents were purified by common methods before utilization. Europium and terbium nitrates were obtained by dissolving lanthanide oxides in concentrated nitric acid.

2.2. Synthesis of precursors

Four precursors were prepared according to the procedures depicted in Fig. 1, using 2-mercaptonicotinic acid (T) as starting reagent. The modifications were performed by addition of 3-methacryloyloxypropyltrimethoxysilane (S_1), 3-glycidoxypropyltrimethoxysilane (S_2), 3-aminopropyltrimethoxysilane (S_3), and 3-(triethoxysilyl)propylisocyanate (S_4), respectively (see Fig. 1A).

2.2.1. Modification by 3-methacryloyloxypropyltrimethoxysilane

0.621 g (4 mmol) 2-mercaptonicotinic acid was first dissolved in 15 mL toluene by stirring and then 0.994 g (4 mmol) 3-methacryloyloxypropyltrimethoxysilane was added to the solution by drops. Three drops of triethylamine was added as catalyzer. The whole mixture was refluxing at 60 °C for 4 h. After isolation, a yellow viscous liquid was obtained and it was named of P_1 in this paper (see Fig. 1A).

2.2.2. Modification by 3-glycidoxypropyltrimethoxysilane

0.621 g (4 mmol) 2-mercaptonicotinic acid was first dissolved in 15 mL pyridine by stirring and then 0.945 g (4 mmol) 3-glycidoxypropyltrimethoxysilane was added to the solution by drops. The whole mixture was refluxing at 80 °C for 4 h. After being condensed to evaporate the solvent and dried on a vacuum line under argon atmosphere, the solution turned to be yellow oil and it was named of P_2 in this paper (see Fig. 1A).

2.2.3. Modification by 3-aminopropyltrimethoxysilane

0.621 g (4 mmol) 2-mercaptonicotinic acid was first dissolved in 15 mL pyridine by stirring and then 0.884 g (4 mmol) 3-aminopropyltrimethoxysilane was added to the solution by drops. The whole mixture was refluxing at 100 °C for 6 h. After filtration, the solution was then condensed to evaporate the solvent. The residue was dried on a vacuum line and yellow oil was obtained and it was named of P_3 in this paper (see Fig. 1A).

2.2.4. Modification by 3-(triethoxysilyl)propylisocyanate

0.621 g (4 mmol) 2-mercaptonicotinic acid was first dissolved in 15 mL pyridine by stirring and then 0.988 g (4 mmol) 3-(triethoxysilyl)propylisocyanate was added to the solution by drops. The whole mixture was refluxing at 80 °C for 3 h. After being condensed to evaporate the solvent and dried on vacuum line under

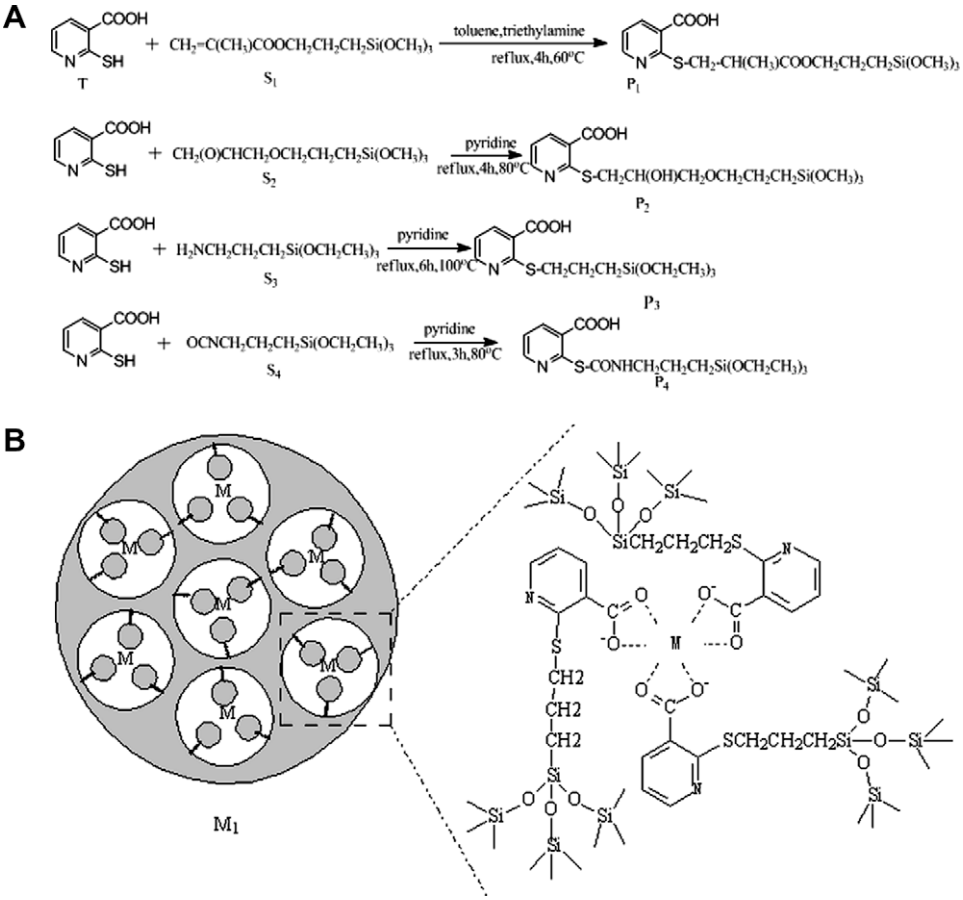

Fig. 1. Scheme for (A) the synthesis of four precursors on the modification of 2-mercaptonicotinic acid and (B) the predicted structure of the hybrid materials.

argon atmosphere, yellow oil was obtained and it was named of P_4 in this paper (see Fig. 1A).

2.3. Synthesis of the hybrid materials

1.0 mmol sulfonamide precursor (P_1 for example) was dissolved in the mixture of 5 mL DMF and 2 mL ethanol by stirring. Then 0.3 mmol $Eu(NO_3)_3{\cdot}6H_2O$ and 2.0 mmol tetraethoxysilane (TEOS) was added into the solution to enhance the sol–gel process. One drop of diluted hydrochloric acid was put into it to promote hydrolysis. The mixture was agitated magnetically in a covered Teflon beaker for an hour. After that, it was aged at 60 °C for the gelation in 3 days. The gels were collected and ground as powder materials for the properties study. The europium hybrids can be named as Eu–M_i (i = 1–4). When $Eu(NO_3)_3{\cdot}6H_2O$ was replaced by $Tb(NO_3)_3{\cdot}6H_2O$, $Zn(AC)_2{\cdot}2H_2O$ in the reagents, another two series of hybrid materials could be prepared (Fig. 1B).

2.4. Physical measurement

Fourier transform infrared (FTIR) spectra were measured within the 4000–400 cm^{-1} region on an (Nicolet Nexus 912 AO446) infrared spectrophotometer with the KBr pellet technique. Ultraviolet absorption spectra were recorded with an Agilent 8453 spectrophotometer. Scanning electronic microscope (SEM) images were obtained with a Philps XL-30. Luminescence (excitation and emission) spectra of these solid complexes were determined with a RF-5301 spectrophotometer. Luminescence lifetime measurements were carried out on an Edinburgh FLS920 phosphorimeter using a 450 W xenon lamp as excitation source. The X-ray diffraction (XRD) measurements were carried out on powdered samples via a "BRUKER D8" diffractometer (40 mA–40 kV) using monochromated Cu Kα_1 radiation (λ = 1.54 Å) over the 2θ range of 10–70°.

3. Results and discussion

3.1. Physical characterizations of the functional sulfide molecular bridge

The FTIR spectra for 2-mercaptonicotinic acid (T), selected precursor (P_2) and the hybrid material (Tb–M_2) are presented in Fig. 2. The modifying reaction of 2-mercaptonicotinic acid can be evidenced by the vanishing of the ν(S–H) at 2196 cm^{-1} and an increase of ν(C–S–C) at 695–655 cm^{-1}. The complete grafting reaction was also proved by two adjacent sharp peaks at 2952 cm^{-1} and 2847 cm^{-1} in curve of the precursor. These two peaks due to ν_{as} (CH_2) and ν_s (CH_2) of the long carbon chain in precursor. The stretching vibration (υSi–O) located at around 1091 cm^{-1} and the stretching vibration (υSi–C) located at 1213 cm^{-1} existed in the spectra of hybrid material (Tb–M_2) which is the evidence of the emergence of Tb–M_2. The broad absorption band at 1200–1100 cm^{-1} (ν(Si–O–Si)) indicated the formation of siloxane bonds. The containing of the organic groups by the silicate inorganic host which occurred in the hydrolysis and condensation process caused the decrease of other peaks' intensities.

The infrared spectroscopy can also prove the coordination of Ln^{3+} ions by the ligands. The $\nu(COO^-)$ vibrations is shifted to lower frequencies ($\triangle\nu$ = 40–70 cm^{-1}) after coordination to the metallic ion with the oxygen atom of the carbonyl group. In spectra of precursor (P_2), the $\nu(COO^-)$ vibration is located at 1441 cm^{-1}. But in the spectra of the hybrid material (Tb–M_2), the $\nu(COO^-)$ vibration is shifted to the 1384 cm^{-1}. The shift is a proof of the coordination of the carboxylic group to the metallic ion with the oxygen atoms.

Fig. 3 shows the UV absorption spectra of 2-mercaptonicotinic acid (T) and four precursors (P_1–P_4). In the five curves, the absorption bands corresponded to the $\pi \rightarrow \pi^*$ electronic transition of aromatic carboxylic acids (K strip) all located at 250 nm. But the absorption peaks corresponded to the $n \rightarrow \pi^*$ electronic transition of sulfide group (R strip) locate at different wavelength. There was a red shift of the $n \rightarrow \pi^*$ electronic transitions (from 292 to 304 nm) comparing the precursors to 2-mercaptonicotinic acid (T). Besides, there was a change of molar absorbance at around 300 nm. All these indicated the modification of the mercapto because the modifications influence the energy difference levels among electron transitions.

3.2. Physical characterizations of the hybrid materials

Fig. 4 shows the XRD patterns of the europium hybrid materials. It reveals that these hybrid materials are totally amorphous. Broad signals are observed ascribed to the short-range order in the materials. These broad signals centered on 26.15° for Eu–M_1, 25.22° for Eu–M_2, 24.14° for Eu–M_3 and 26.90° for Eu–M_4 in the XRD patterns because of the coherent diffraction of the siliceous backbone in the hybrids. The presence of organic part in the inorganic framework leads to the absence of any crystalline regions in these samples.

The scanning electron micrographs of Eu–M_1, Eu–M_2, Tb–M_3, Tb–M_4 are shown in Fig. 5. From these images for the hybrid mate-

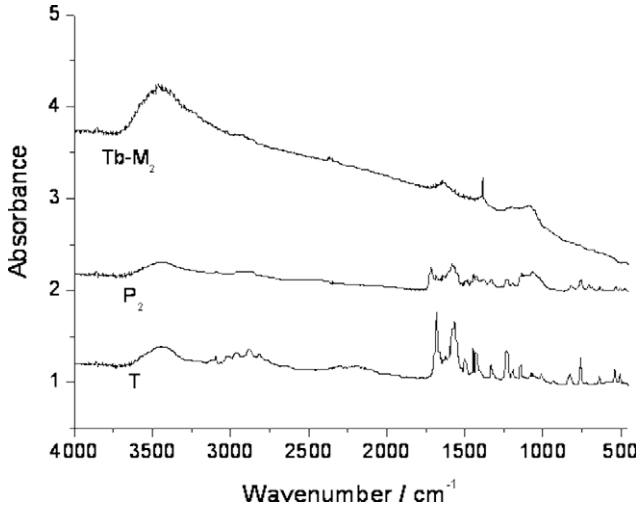

Fig. 2. The selected FTIR spectra for 2-mercaptonicotinic acid (T), P_2 and Tb–M_2.

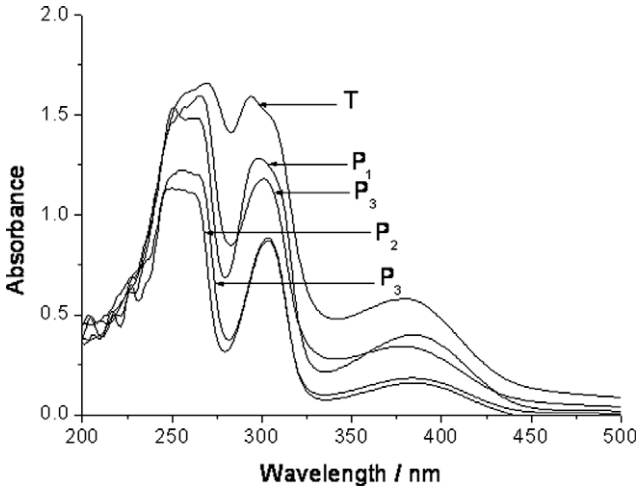

Fig. 3. Ultraviolet absorption spectra of 2-mercaptonicotinic acid (T) and four precursors (P_1–P_4).

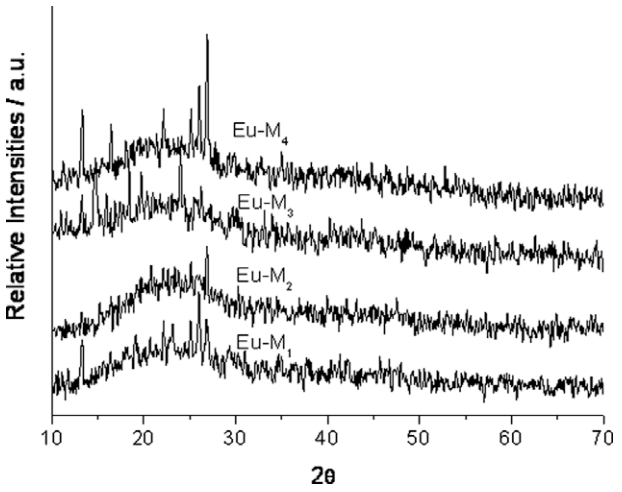

Fig. 4. X-ray diffraction (XRD) graphs of the hybrid material Eu–M_i (i = 1–4).

rials it can be concluded that homogeneous, molecular-based materials were obtained where no phase separation was observed because of strong covalent bonds bridging between the inorganic and organic phases. On the surface of these hybrid materials, uniform spherical or clubbed particles can be observed. These phenomena are mostly owing to the sol–gel treatment. Five milliliters of DMF and 2 mL ethanol were chosen as the solution, and the precursors; Lanthanide nitrate; TEOS were all dissolved in it. The mixture was agitated magnetically to achieve a single phase, and this process made the ethanol uniformly dispersed in the DMF to form small drips. During the gelation process the reaction occurred in these small drips. Rudimental solutions were released from the surface of these drips. Meanwhile the inorganic skeleton has been formed because of the formation of Si–O bonds. Finally the uniform spherical or clubbed particles on the surface of the hybrid materials can be observed. As mentioned in Section 2, the hybrid materials could be received through a polycondensation reaction between the terminal silanol groups of Ln(Zn)–M_i and the OH groups of hydrolyzed TEOS. At the beginning of the reaction, the individual hydrolysis of Ln(Zn)–M_i and TEOS are predominant. Subsequent process is related to the polycondensation reactions between hydroxyl groups of both Ln(Zn)–M_i and TEOS. By these methods, the covalently bonded hybrids can be achieved. Here we named the cooperation of both Ln(Zn)–M_i and TEOS within the in situ sol–gel process as cohydrolysis and copolycondensation (similar to copolymerization of organic monomer). All the functional molecular bridges derive from the sulfide of T with P_1–P_5 and the carboxylate group is kept, so the coordination behavior mainly depends on carboxylate group. Different hybrids derived different sulfide linkages have apparent influence on the micromorphology.

3.3. Photophysical properties

The low temperature phosphorescence spectra of 2-mercaptonicotinic acid (M) and the four derived precursors (S_1–S_4) are recorded and the triplet state energies of them can be determined. The red shifts as above are observed between T and precursors except for P_1–P_4, suggesting conjugate groups have been modified for the modification. The energy differences (ΔE) between the triplet state energy levels and the resonant emissive energy levels of Ln^{3+} (Ln = Eu, Tb) can be taken at the maximum of emission and are reported in Table 1. According to the energy transfer and intramolecular energy mechanism [28–30], the intramolecular energy migration efficiency from organic ligands to the central Ln^{3+} is the most important factor to determine the luminescence properties of lanthanide complexes [54]. The intramolecular energy transfer efficiency is established mainly on two energy transfer processes [31,32]. One is from the triplet state energy of organic ligands to the resonant energy level by Dexter's resonant exchange interaction theory [31], the other is the inverse energy transition by thermal deactivation mechanism [32]. It can be concluded that the much overlap between the luminescence spectrum of organic

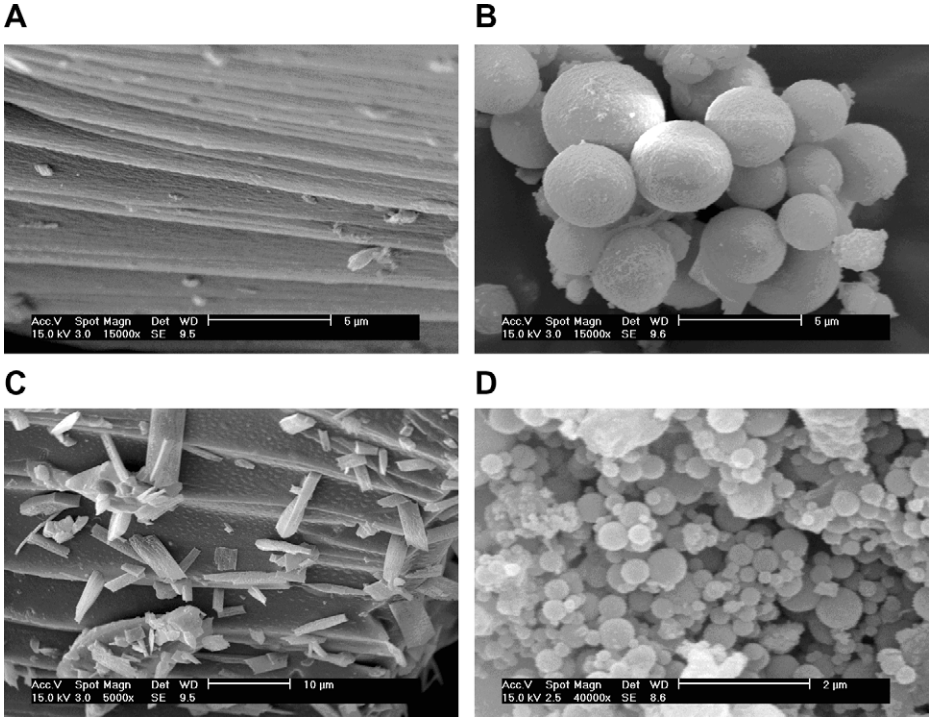

Fig. 5. Selected scanning electron micrographs (SEM) of Eu–M_1 (A), Eu–M_2 (B), Tb–M_3 (C), Tb–M_4 (D).

Table 1
The triplet state energies of molecular bridges and their energy transfer with lanthanides ions.

Complexes	λ_{max} (nm)	Triplet state energies (cm^{-1})	ΔE(Tr–Eu^{3+}) (cm^{-1})	ΔE(Tr–Tb^{3+}) (cm^{-1})
M	451	22 170	4870	2120
S_1	458	21 835	4535	1335
S_2	462	21 645	4345	1145
S_3	465	21 505	4205	1005
S_4	473	21 140	3840	640

ligands can both enhance the two process. So there should exist an optimal energy difference between the triplet state position of organic ligands and the emissive energy level of Ln^{3+} ions. The following emission spectra obtained from Tb and Eu hybrids further demonstrate our predicted conclusion.

Fig. 6 shows the selected UV–Vis DRS of Eu–M_3, Tb–M_2. Both have broad absorption band ranging from 200 to 480 nm. The broad absorption may owe to the presence of organic part in the inorganic framework. And the broad absorption band in the short wavelength region lead to the good luminescence properties of these hybrid materials. The negative absorption peak corresponds to the characteristic emission peak at 613 nm of the active europium ions can be observed in the spectrum of Eu–M_3. The spectrum of Tb–M_2 shows that the negative absorption peak is the characteristic emission peak at 545 nm of the active terbium ions. Compared them with the absorption spectra of bridge precursors (Fig. 3 (P_3, P_2), it can be seen that the hybrids show the much wider absorption than the corresponding linkage, suggesting the formation of Si–O network and introduction of Eu or Tb ions are benefit for the absorption and energy transfer for the luminescence of Eu or Tb ions in the hybrid materials systems. Besides, there exist difference between Eu–M_3 and Tb–M_2, which is due to the similar above reason. The different lanthanide ions and different organo-modified Si–O network have great influence on the absorption of hybrid systems.

The emission spectra of the europium hybrid materials are shown in Fig. 7. The strong red luminescence was observes in their emission spectra, which indicated that the effective energy transfer took place between the aromatic ligand and the chelated Eu^{3+} ions. The emission line of the hybrid materials was assigned to the $^5D_0$–^7F_J (J = 1–4) transitions at around 588, 613, 649, 683 nm, respectively. Besides, There exists apparent emission in the short wavelength region of 450–550 nm, which may be ascribed to the emission of the Si–O network. The maxima of these bands are at around 588 and 613 nm. A prominent phenomenon that should be noticed in these spectra is the very high intensity of the $^5D_0 \rightarrow {}^7F_2$ transition. $^5D_0 \rightarrow {}^7F_1$ transition is magnetic-dipolar transitions and insensitive to their local structure environment while $^5D_0 \rightarrow {}^7F_2$ transition is electric-dipolar transitions and sensitive to the coordination environment of the Eu^{3+} ion. Stronger the interactions of the rare-earth complex with its local chemical environment are, more nonsymmetrical the complex becomes. And the electric-dipolar transitions become more intense. As a result, the intensity ratio of the $^5D_0 \rightarrow {}^7F_2$ transition to $^5D_0 \rightarrow {}^7F_1$ transition has been widely used as an indicator of Eu^{3+} site symmetry. In these europium hybrid materials, from M_1 to M_4, the intensity ratios I_{02} ($^5D_0 \rightarrow {}^7F_2$)/$I_{01}$ ($^5D_0 \rightarrow {}^7F_1$) are 2.34, 2.83, 2.95 and 2.51, respectively. This ratio is only possible when the europium ion does not occupy a site with inversion symmetry [33,28,34].

Fig. 8 illustrates typical photoluminescence spectra of the terbium hybrid materials. The emission lines of these hybrid materials can be assigned to the transitions from the $^5D_4 \rightarrow {}^7F_J$ (J = 6, 5, 4, 3) transitions at around 488, 543, 582 and 620 nm, respectively, for terbium ions. Among these emission peaks, the most striking green luminescence ($^5D_4 \rightarrow {}^7F_5$) and blue luminescence ($^5D_4 \rightarrow {}^7F_6$) can be observed in their emission spectra, which indicates that the effective energy transfer process has taken place between the ligands and the chelated Tb^{3+} ions. The green emission is stronger than that of the blue one. The reason may be that the emission to $^5D_4 \rightarrow {}^7F_6$ is mainly an electronic dipole transition, which is greatly influenced by the ligand field, while the emission to $^5D_4 \rightarrow {}^7F_5$ belonging to mainly a magnetic dipole transition, which is less influenced by the ligand field [35]. Besides, these bands in the short wavelength region cannot be clearly found in the spectra of terbium hybrids, suggesting that there exist more effective energy transfer process in the terbium hybrids than europium ones.

Fig. 9 shows the emission spectra of the zinc hybrid materials. The luminescence principle of zinc hybrids is different from that of lanthanide molecular hybrids. Lanthanide molecular hybrids based on the intramolecular energy transfer between ligand sys-

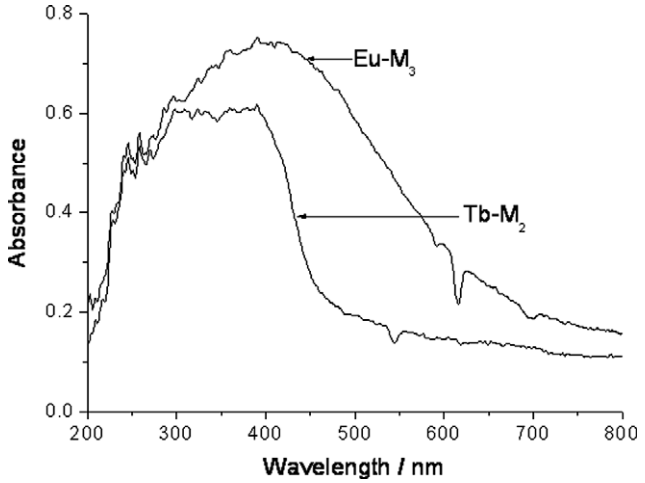

Fig. 6. UV–Vis DRS spectra of Eu–M_3, Tb–M_2.

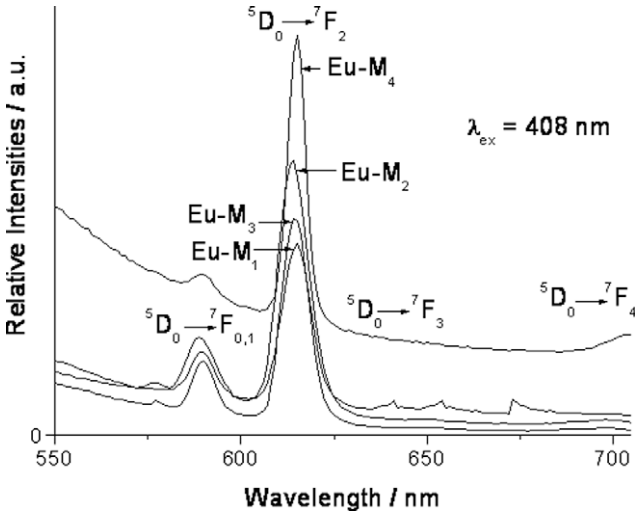

Fig. 7. Emission spectra of europium hybrid materials.

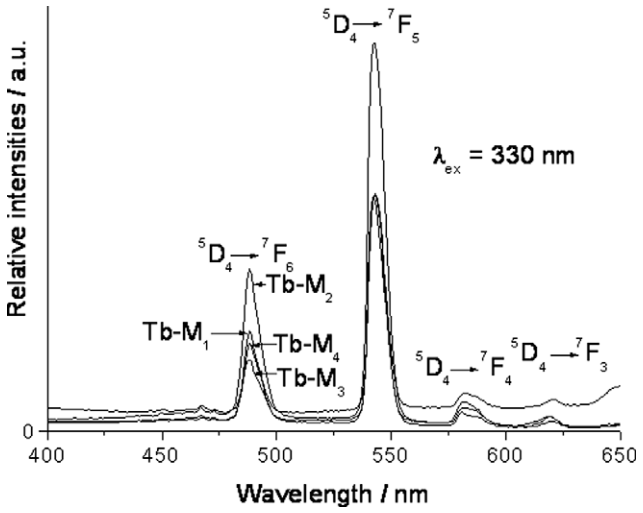

Fig. 8. Emission spectra of terbium hybrid materials.

tems to Ln^{3+}, but the luminescence zinc molecular hybrid systems derived from the ligands are influenced by the disturbance of Zn^{2+}. All four zinc hybrids show violet emission at around 360 nm. The emission ascribed to the Si–O network in the short wavelength region of 450–500 nm can also be observed in these emission spectra of the zinc hybrids.

The typical decay curve of the Eu^{3+} hybrid materials were measured and they can be described as a single exponential ($\mathrm{Ln}(S(t)/S_0) = -k_1 t = -t/\tau$), indicating that all Eu^{3+} ions occupy the same average coordination environment. The resulting lifetime data of Eu^{3+} hybrid materials are given in Table 2. Further, we selectively determined the emission quantum efficiencies of the $^5D_0$ excited state of europium ion for Eu^{3+} hybrids on the basis of the emission spectra and lifetimes of the $^5D_0$ emitting level, the detailed luminescent data are shown in Table 2. The quantum efficiency of the luminescence step, η expresses how well the radiative processes (characterized by rate constant A_r) compete with non-radiative processes (overall rate constant A_{nr}) [36–42]

$$\eta = A_r/(A_r + A_{nr}) \quad (1)$$

Non-radiative processes influence the experimental luminescence lifetime by the equation:

$$\tau_{exp} = (A_r + A_{nr})^{-1} \quad (2)$$

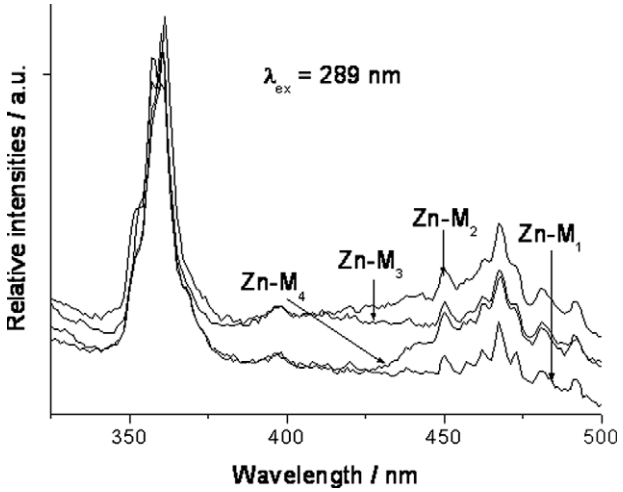

Fig. 9. Emission spectra of zinc hybrid materials.

Table 2
The luminescence efficiencies and lifetimes of the europium covalent hybrids.

Systems	Eu–M_1	Eu–M_2	Eu–M_3	Eu–M_4
τ (ms)	0.45	0.80	0.52	0.66
υ_{01} (cm^{-1}) [a]	16 978	16 980	16 958	16 939
υ_{02} (cm^{-1}) [a]	16 268	16 284	16 268	16 268
υ_{03} (cm^{-1}) [a]	15 313	15 314	15 429	15 307
υ_{04} (cm^{-1}) [a]	14 859	14 342	14 361	14 206
I_{01} [b]	128.09	148.03	109.76	242.25
I_{02} [b]	291.01	415.45	329.70	606.74
I_{03} [b]	50.78	25.56	14.12	140.23
I_{04} [b]	52.36	23.87	11.59	154.16
A_{01} (s^{-1})	50	50	50	50
A_{02} (s^{-1})	118.55	146.32	156.56	130.39
A_{03} (s^{-1})	21.97	9.57	7.07	32.03
A_{04} (s^{-1})	23.35	9.55	6.24	37.94
A_{rad} (s^{-1})	213.87	215.44	219.87	250.36
η (%)	9.7	17.2	11.4	16.5

[a] The energies of the $^5D_0 \rightarrow {}^7F_J$ transitions (υ_{0J}).
[b] The integrated intensity of the $^5D_0 \rightarrow {}^7F_J$ emission curves.

So quantum efficiency can be calculated from radiative transition rate constant and experimental luminescence lifetime from the following equation:

$$\eta = A_r \tau_{exp} \quad (3)$$

where A_r can be obtained by summing over the radiative rates A_{0J} for each $^5D_0 \rightarrow {}^7F_J$ transitions of Eu^{3+}

$$A_r = \sum A_{0J} = A_{00} + A_{01} + A_{02} + A_{03} + A_{04} \quad (4)$$

The branching ratio for the $^5D_0 \rightarrow {}^7F_{5,6}$ transitions can be neglected as they both are not detected experimentally, whose influence can be ignored in the depopulation of the $^5D_0$ excited state. Since $^5D_0 \rightarrow {}^7F_1$ belongs to the isolated magnetic dipole transition, it is practically independent of the chemical environments around the Eu^{3+} ion, and thus can be considered as an internal reference for the whole spectrum, the experimental coefficients of spontaneous emission, A_{0J} can be calculated according to the equation

$$A_{0J} = A_{01}(I_{0J}/I_{01})(U_{01}/U_{0J}) \quad (5)$$

Here A_{0J} is the experimental coefficients of spontaneous emissions, among A_{01} is the Einstein's coefficient of spontaneous emission between the $^5D_0$ and $^7F_1$ energy levels. In vacuum, A_{01} as a value of 14.65 s^{-1}, when an average index of refraction n equal to 1.506 was considered, the value of A_{01} can be determined to be 50 s^{-1} approximately ($A_{01} = n^3 A_{01\ (vacuum)}$). I is the emission intensity and can be taken as the integrated intensity of the $^5D_0 \rightarrow {}^7F_J$ emission bands. υ_{0J} refers to the energy barycenter and can be determined from the emission bands of Eu^{3+}'s $^5D_0 \rightarrow {}^7F_J$ emission transitions. Here the emission intensity, I, taken as integrated intensity S of the $^5D_0 \rightarrow {}^7F_{0-4}$ emission curves, can be defined as below:

$$I_{i-j} = \hbar\omega_{i-j} A_{i-j} N_i \approx S_{i-j} \quad (6)$$

where i and j are the initial ($^5D_0$) and final levels ($^7F_{0-4}$), respectively, ω_{i-j} is the transition energy, A_{i-j} is the Einstein's coefficient of spontaneous emission, and N_i is the population of the $^5D_0$ emitting level. On the basis of the above discussion, the quantum efficiencies of the five kinds of europium polymeric hybrid materials can be determined in the order: Eu–M_2 > Eu–M_4 > Eu–M_3 > Eu–M_1, which take agreement with the order of lifetimes. From the equation of η, it can be seen the value η mainly depends on the values of two quantum: lifetimes and red/orange ratio (I_{02}/I_{01}). If the lifetimes and red/orange ratio are large, the quantum efficiency must be high. So the different composition of the hybrid materials may have influence on the luminescent lifetimes and quantum efficiencies.

Besides, the 1:1 molar ratio of Ln^{3+} and Cali-Si can be predicted with content of Ln in covalently bonded hybrid materials. In order

to study the coordination environment surround lanthanide ions especially the influence caused by vibrations of water molecules, according to Horrocks' previous research [43,44], it is therefore expected that probable number of coordinated water molecules (n_w) can be calculated as following equation:

$$n_w = 1.05(A_{exp} - A_{rad}) \quad (7)$$

in which A_{rad} and A_{nrad} are radiative and nonradiative probabilities, respectively. τ_{exp} is decay time of Eu containing covalent hybrids. A_{rad} can be described as the ratio of relative intensities of $^5D_0 \rightarrow {}^7F_J$ (J = 1, 2, 3, 4) transitions. The values of A_{rad}, A_{nrad} and n_w were calculated through the above three equations and reported in Table 1. Based on the results, the coordination number of water molecules (Eu containing hybrid materials) can be estimated to be six. The coordinated water molecules produce the severe vibration of hydroxyl group, resulting in the large non-radiative transition and decreasing the luminescent efficiency.

4. Conclusions

In summary, by means of the molecular modification of aromatic carboxylic acid with mercapto (2-mercaptonicotinic acid) with four different modified alkoxysilanes, four kinds of structural molecular bridges were designed to obtain double reactivity. Further, four molecular bridges and lanthanides (europium and terbium) and zinc ions were successfully assembled. A series of molecular hybrid materials with strong chemical bonds were constructed, which show the characteristic luminescence and uniform microstructure. The ideal physical, chemical and luminescent properties of the hybrids showed that the modification of the 2-mercaptonicotinic acid is practical, which can be easily applied to other organic compounds and to different modified alkoxysilanes.

Acknowledgements

This work was supported by the National Natural Science Foundation of China (20671072) and Program for New Century Excellent Talents in University NCET-08-0398.

References

[1] T. Suratwala, Z. Gardlund, K. Davidson, D.R. Uhlmann, Chem. Mater. 10 (1998) 190–198.
[2] G. Blasse, B.C. Grabmaier, Luminescent Materials, Springer, Berlin, 1994.
[3] L.R. Matthews, E.T. Knobbe, Chem. Mater. 5 (1993) 1697–1700.
[4] P.A. Tanner, B. Yan, H.J. Zhang, J. Mater. Sci. 35 (2000) 4325–4329.
[5] Q.H. Xu, L.S. Li, X.S. Liu, R.R. Xu, Chem. Mater. 14 (2002) 549–555.
[6] C. Sanchez, F. Ribot, New J. Chem. 18 (1994) 1007–1047.
[7] A.C. Franville, D. Zambon, R. Mahiou, Y. Troin, Chem. Mater. 12 (2000) 428–435.
[8] H.R. Li, J. Lin, H.J. Zhang, H.C. Li, L.S. Fu, Q.G. Meng, Chem. Commun. 13 (2001) 1212–1213.
[9] D.W. Dong, S.C. Jiang, Y.F. Men, X.L. Ji, B.Z. Jiang, Adv. Mater. 12 (2000) 646–649.
[10] Q.M. Wang, B. Yan, J. Mater. Chem. 14 (2004) 2450–2455.
[11] Q.M. Wang, B. Yan, J. Photochem. Photobiol. A: Chem. 178 (2006) 70–75.
[12] Q.M. Wang, B. Yan, Cryst. Growth Des. 5 (2005) 497–503.
[13] Q.M. Wang, B. Yan, J. Mater. Res. 20 (2005) 592–598.
[14] Q.M. Wang, B. Yan, J. Photochem. Photobiol. A: Chem. 175 (2006) 159–165.
[15] Q.M. Wang, B. Yan, J. Organomet. Chem. 691 (2006) 540–545.
[16] B. Yan, D.J. Ma, J. Solid State Chem. 179 (2006) 2059–2066.
[17] B. Yan, X.F. Qiao, Photochem. Photobiol. 83 (2007) 971–978.
[18] B. Menaa, M. Takahashi, Y. Tokuda, T. Yoko, Opt. Mater. 29 (2007) 806–813.
[19] M.R. Casalboni, P. Senesi, Appl. Phys. Lett. 30 (1997) 2969–2971.
[20] B. Lebeau, C.E. Fowler, S.R. Hall, S. Mann, J. Mater. Chem. 9 (1999) 2279–2281.
[21] P. Innocenzi, H. Kozuka, T. Yoko, J. Phys. Chem. B 101 (1997) 2285–2291.
[22] K. Mstsui, F. Momose, Chem. Mater. 9 (1997) 2588–2591.
[23] S. Vijaikumar, K. Pitchumani, J. Mol. Catal. A: Chem. 17 (2004) 117–120.
[24] L.N. Nikolenko, V.A. Koptyug, Z. Obshchei Khim. 25 (1955) 1757–1760.
[25] M. Bandini, P.G. Cozzi, M. Giacomini, P. Melchiorre, S. Selva, A. Umani-Ronchi, J. Org. Chem. 67 (2002) 3700–3704.
[26] F. Fringuelli, F. Pizzo, C. Vittoriani, L. Vaccaro, Eur. J. Org. Chem. 5 (2006) 1231–1236.
[27] G. Tarzia, A. Duranti, A. Tontini, G. Piersanti, M. Mor, S. Rivara, P.V. Plazzi, C. Park, S. Kathuria, D. Piomelli, J. Med. Chem. 46 (2003) 2352–2360.
[28] M.H.V. Werts, R.T.F. Jukes, J.W. Verhoeven, Phys. Chem. Chem. Phys. 4 (2002) 1542–1548.
[29] S. Sato, M. Wada, Bull. Chem. Soc. Jap. 43 (1970) 1955–1966.
[30] Q.M. Wang, B. Yan, X.H. Zhang, J. Photochem. Photobiol. A: Chem. 174 (2005) 119–124.
[31] D.L. Dexter, J. Chem. Phys. 21 (1953) 836–839.
[32] C.R.S. Dean, T.M. Shepherd, J. Chem. Soc., Faraday Trans. II 71 (1975) 146–150.
[33] Y. Hasegawa, M. Yamamuro, Y. Wada, N. Kanehisa, Y. Kai, S. Yanagida, J. Phys. Chem. A 107 (2003) 1697–1702.
[34] K. Binnemans, K. Van Herck, C. Gorller-Walrand, Chem. Phys. Lett. 266 (1997) 297–302.
[35] B.L. An, M.L. Gong, K.Y. Cheah, W.K. Wong, J.M. Zhang, J. Alloys Compd. 368 (2004) 326–332.
[36] L.D. Carlos, Y. Messaddeq, H.F. Brito, R.A.S. Ferreira, V.D. Bermudez, S.J.L. Ribeiro, Adv. Mater. 12 (2000) 594–598.
[37] P.C.R. Soares-Santos, H.I.S. Nogueira, V. Felix, M.G.B. Drew, R.A.S. Ferreira, L.D. Carlos, T. Trindade, Chem. Mater. 15 (2003) 100–108.
[38] E.E.S. Teotonio, J.G.P. Espinola, H.F. Brito, O.L. Malta, S.F. Oliveria, D.L.A. de Faria, C.M.S. Izumi, Polyhedron 21 (2002) 1837–1844.
[39] S.J.L. Ribeiro, K. Dahmouche, C.A. Ribeiro, C.V. Santilli, S.H.J. Pulcinelli, J. Sol–Gel Sci. Technol. 13 (1998) 427–430.
[40] O.L. Malta, M.A.C. dosSantos, L.C. Thompson, N.K. Ito, J. Lumin. 69 (1996) 77–84.
[41] G.F. de Sa, O.L. Malta, C.D. Donega, A.M. Simas, R.L. Longo, P.A. Santa-Cruz, E.F. da Silva, Coord. Chem. Rev. 196 (2000) 165–196.
[42] J.C. Boyer, F. Vetrone, J.A. Capobianco, A. Speghini, M. Bettinelli, J. Phys. Chem. B 108 (2004) 20137–20144.
[43] W.De W. Horrocks, D.R. Sudnick, J. Am. Chem. Soc. 101 (1979) 334–340.
[44] W. De W. Horrocks, D.R. Sudnick, Acc. Chem. Res. 14 (1981) 384–392.